First Octahedral Spherical Hohlraum Energetics Experiment at the SGIII Laser Facility

Wen Yi Huo,[1,*] Zhichao Li,[2,3] Yao-Hua Chen,[1] Xufei Xie,[2] Guoli Ren,[1] Hui Cao,[1] Shu Li,[1] Ke Lan,[1,3,4,†] Jie Liu,[1,3,4]
Yongsheng Li,[1] Sanwei Li,[2] Liang Guo,[2] Yonggang Liu,[2] Dong Yang,[2] Xiaohua Jiang,[2] Lifei Hou,[2] Huabing Du,[2]
Xiaoshi Peng,[2] Tao Xu,[2] Chaoguang Li,[2] Xiayu Zhan,[2] Zhebin Wang,[2] Keli Deng,[2] Qiangqiang Wang,[2] Bo Deng,[2]
Feng Wang,[2] Jiamin Yang,[2] Shenye Liu,[2] Shaoen Jiang,[2] Guanghui Yuan,[2] Haijun Zhang,[2] Baibin Jiang,[2] Wei Zhang,[2]
Qianqian Gu,[2] Zhibing He,[2] Kai Du,[2] Xuewei Deng,[2] Wei Zhou,[2] Liquan Wang,[2] Xiaoxia Huang,[2] Yuancheng Wang,[2]
Dongxia Hu,[2] Kuixing Zheng,[2] Qihua Zhu,[2] and Yongkun Ding[2,3]

[1]*Institute of Applied Physics and Computational Mathematics, Beijing 100088, China*
[2]*Research Center of Laser Fusion, Chinese Academy of Engineering Physics, Mianyang 621900, China*
[3]*Collaborative Innovation Center of IFSA, Shanghai Jiao Tong University, Shanghai 200240, China*
[4]*Center for Applied Physics and Technology, Peking University, Beijing 100871, China*

The first octahedral spherical hohlraum energetics experiment is accomplished at the SGIII laser facility. For the first time, the 32 laser beams are injected into the octahedral spherical hohlraum through six laser entrance holes. Two techniques are used to diagnose the radiation field of the octahedral spherical hohlraum in order to obtain comprehensive experimental data. The radiation flux streaming out of laser entrance holes is measured by six flat-response x-ray detectors (FXRDs) and four *M*-band x-ray detectors, which are placed at different locations of the SGIII target chamber. The radiation temperature is derived from the measured flux of FXRD by using the blackbody assumption. The peak radiation temperature inside hohlraum is determined by the shock wave technique. The experimental results show that the octahedral spherical hohlraum radiation temperature is in the range of 170–182 eV with drive laser energies of 71 kJ to 84 kJ. The radiation temperature inside the hohlraum determined by the shock wave technique is about 175 eV at 71 kJ. For the flat-top laser pulse of 3 ns, the conversion efficiency of gas-filled octahedral spherical hohlraum from laser into soft x rays is about 80% according to the two-dimensional numerical simulation.

The laser indirect drive inertial confinement fusion (ICF) uses a hohlraum to convert laser energy into soft x rays. The radiation drive provided by the hohlraums must be intense and symmetric enough in order to compress the capsule with D-T fuel to ignition [1,2]. While many important progresses in ICF have been achieved at the National Ignition Facility (NIF) [3–10] and on OMEGA [11–14], ignition has not yet been demonstrated. The integrated experiments at the NIF show that radiation asymmetry is one of the main obstacles in achieving ignition [15–21].

The octahedral spherical hohlraum [22–26] has natural superiority in providing high radiation symmetry and attracts much research interest [27]. Recently, we have accomplished many important experiments to investigate the performance of spherical hohlraums by using a spherical hohlraum with two laser entrance holes (LEHs), such as the laser spot movement experiment [28,29], the experiment demonstrating weak laser plasma instabilities in gas-filled spherical hohlraums [30,31], and the energetics experiment [32]. However, one of the crucial issues, that is the energetics of octahedral spherical hohlraum with six LEHs, has not been investigated. In hohlraum energetics study, the intensity of the radiation field and the conversion

efficiency from laser to x rays are two key issues. The intensity of a hohlraum radiation field determines how to design and perform the integrated experiments on the laser facility. The conversion efficiency is directly related to the energy scale of the ignition laser facility. There have been a great deal energetics experiments performed at several different laser facilities, such as NOVA [33,34], OMEGA [35], SGIII-P [36–38], and NIF [39–42], for investigating the two important issues of cylindrical hohlraums.

There are several scientific and technical challenges in performing the octahedral spherical hohlraum energetics experiment at the laser facilities designed for the cylindrical hohlraum with two LEHs. First, the pattern of the laser entering into the hohlraum must be redesigned so that the laser beams can be injected into the octahedral spherical hohlraum through six LEHs. How to keep the laser pointing accuracy in the new laser injection fashion must be investigated experimentally. Second, the fabrication of a octahedral spherical hohlraum is a new area for target fabrication, because the current fabrication technique is developed for axial symmetric cylindrical hohlraums. The assemblage and pointing of an octahedral spherical hohlraum in the target chamber is also a challenge. Third, the

diagnostic of the radiation field of octahedral spherical hohlraum is a quite difficult issue, and the radiation temperature of an octahedral spherical hohlraum has never been obtained in experiment.

In order to explore the characterization of the radiation field of the octahedral spherical hohlraum, we have performed the energetics experiment of the spherical hohlraum with two LEHs on the SGIII-P [32]. In that experiment, we used the flat x-ray detectors (FXRDs) [43] to measure the radiation flux streaming out of a LEH from different angles, and the radiation temperature and M-band fraction inside the hohlraum is determined by the shock wave technique [37,44]. The success of that experiment inspires us so that we can use the two techniques to diagnose the radiation field of octahedral spherical hohlraum. In this Letter, we report on the first energetics experiment of an octahedral spherical hohlraum with six LEHs performed at the SGIII laser facility and describe how we solve the technical and scientific challenges.

The experiment is conducted at the SGIII laser facility [45] which consists of 48 laser beams at a wavelength of 0.35 μm. The 48 laser beams are arranged into 4 cones for both the lower and upper hemispheres of the target chamber. The two inner cones are at 28.5° and 35° with respect to the vertical axis while the outer cones are at 49.5° and 55°. There are twice as many beams in the outer cones as in the inner cones. The maximum output laser energy is about 180 kJ at 3 ns square laser pulse. Because the SGIII laser facility was designed for cylindrical hohlraums, the laser beams must be reoriented in order to let the laser beams enter the octahedral spherical hohlraum through six LEHs. Considering the laser beam arrangement of the SGIII laser facility, we select 32 of 48 laser beams to drive the octahedral spherical hohlraum. For the upper and lower LEHs, there are eight laser beams entering into the hohlraum, including four 55° laser beams and four 28.5° laser beams, respectively. For the four LEHs at the equatorial plane, there are separately 4 laser beams entering into the hohlraum, including two 50° laser beams and two 35° laser beams. The incident angles of the 50° and 35° laser beams are 47.9° and 61.5°, respectively. In Fig. 1, we present the schematic view of the experimental setup. Prior to the experiment, we evaluate the precision of the laser pointing on the equatorial LEH plane by using the imaging technique to ensure that the laser beams cannot clip the edge of LEHs.

The size of the octahedral spherical hohlraum is designed according to the total drive energy and the laser beam arrangement. The radius of the hohlraum is taken as 2.4 mm, the radius of the LEHs are determined by the size of the laser focal spot. The laser beams are smoothed by the continuous phase plates (CPPs). The CPP produces a circular laser focal spot at the upper and lower LEH planes with a radius of 250 μm. The diameter of upper and lower LEHs is taken as 0.6 mm. However, the laser focal spots at
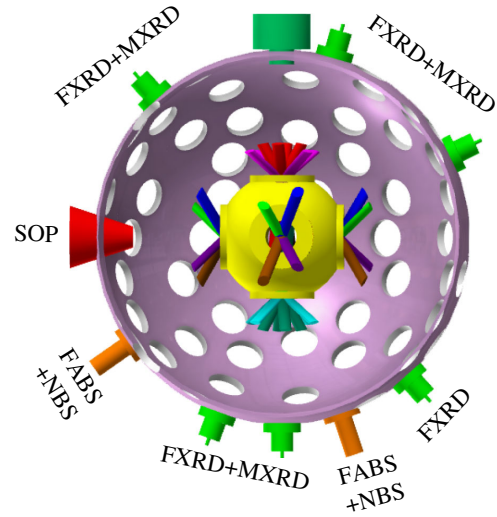
FIG. 1. A schematic view of the experimental setup and arrangement of the main diagnostic devices used in the experiment.

the equatorial LEH plane are elliptical, so the diameter of equatorial LEHs is taken as 0.7 mm in order for the laser beams to be injected into the hohlraum.

It should be pointed out that the octahedral spherical hohlraum used in this experiment cannot produce the same high radiation symmetry as the ignition octahedral spherical hohlraum [22]. First, the laser beam arrangement is not ideal because we use only 32 of 48 laser beams to drive the hohlraum. Second, the sizes of the six LEHs are not the same, and the equatorial LEHs are larger than the polar LEHs. In these circumstances, the radiation flux asymmetry $\Delta F/F$ [22] is in the vicinity of 5% when the ratio of hohlraum radius to capsule radius R_H/R_C ranges from 5 to 7 according to the calculation results of the three-dimensional view factor code VF3D [27]. And the low mode asymmetry P_2 dominates the flux asymmetry. P_2 asymmetry ranges from 2.6% to 3% when R_H/R_C ranges from 7 to 5. The radiation asymmetry is mainly induced by the different sizes of LEHs.

The gas-filled octahedral spherical hohlraum with cylindrical LEHs [24,28] is used in the experiments. The hohlraum is filled with C_5H_{12} at a density 0.9 mg/cc, and the electron density inside the hohlraum is about 5% of the laser critical density when the filled gas C_5H_{12} is fully ionized. The Full Aperture Backscatter Station (FABS) and Near Backscatter Station (NBS) are used to measure the backscatter fraction of the incident laser due to the stimulated Raman scattering (SRS) and the stimulated Brillouin scattering (SBS). There are a total four backscatter measurement stations used to measure the scattered laser energy of one beam of every laser cone at the lower hemisphere. In Fig. 2(a), we present the measured total scattered energies in three shots in which the hohlraum is driven by 32 laser beams. The maximum backscattered energy is lower than 140 J. In the experiment, the driving
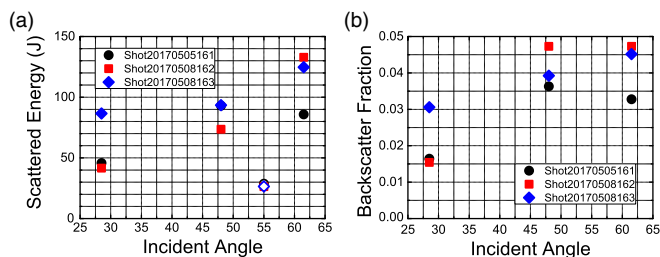
FIG. 2. (a) The total scattered energies of four laser beams at different incident angles. The solid point is the backscattered energy and the hollow point is the sidescattered energy. (b) The backscatter fractions of three laser beams at different incident angles.

energy is about 2.7 kJ/beam. The backscattered fraction due to laser plasma instabilities is lower than 5% although the crossover of laser beams inside the hohlraum is serious, as shown in Fig. 2(b). An interesting phenomenon is that there are energies scattered into the backscatter station of the laser beam at 55° which is not used. However, the measured scattered energy at 55° is mainly from the SBS signal of the NBS.

Based on the success of the previous experiment [32], we use six FXRDs to measure the radiation flux streaming out of the LEHs. The M-band (> 1.6 keV) flux streaming out of the LEHs is measured by four filtered M-band x-ray detectors (MXRDs) [46]. The six FXRDs are installed on different locations of the SGIII target chamber, with three installed on the upper hemisphere at 16°, 42°, and 64°, and three installed on the lower hemisphere at 0°, 20°, and 42°. The locations of FXRDs on the target chamber are carefully designed in order to obtain comprehensive data of the radiation field of the octahedral spherical hohlraum. As shown in Fig. 3, the FXRD at upper 64° sees the most areas of hohlraum interior surface through 3 LEHs, including both the reemission region and the laser spots. The measured flux of the FXRDs at upper 16° and lower 20° comes mainly from the reemission region through one
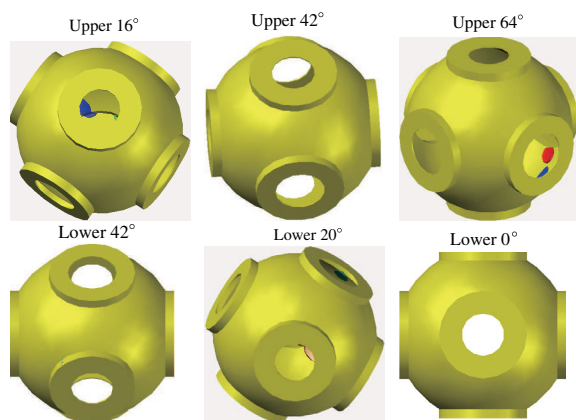
FIG. 3. The view fields of the six FXRDs installed on the different locations of target chamber.

LEH, although there are three LEHs and little laser spot in their view fields. The two FXRDs at upper and lower 42° measure the radiation flux emitted from ablated plasmas between tow adjacent LEHs. The FXRD at lower 0° measures the radiation flux emitted from the plasmas accumulated inside the hohlraum. The four MXRDs are installed at the same place with the FXRDs at upper 16°, 42°, 64°, and lower 0°. In some shots, the radiation temperature inside the hohlraum is determined by the shock wave technique with witness material Al. The stepped witness plate is placed at one equatorial LEH, and a streaked optical pyrometer (SOP) is used to measure the shock velocity in Al.

In Fig. 4(a), we present the temporal radiation fluxes measured by different FXRDs for a hohlraum with 83 kJ drive energy. As shown in Fig. 4(a), the measured flux of the FXRD at upper 64° is the highest and the peak flux is about 700 GW/sr, and at lower 0° is the lowest of about 100 GW/sr. The measured fluxes of the FXRDs at upper 16° and lower 20° are close to each other. The measured flux of the FXRD at upper 42° is slightly higher than that of lower 42°. The experimental observations of total radiation flux can be understood by analyzing the view fields of FXRDs. As shown in Fig. 3, there are three LEHs in the view field of the FXRD at upper 64°, the upper LEH and two equatorial LEHs, and it sees the most areas of hohlraum wall through these LEHs and two laser spots. As a result, the measured flux of the FXRD at upper 64° is the highest. For the same reason, the measured M-band flux of upper 64° is also the highest. The hohlraum wall areas and laser spots in the view fields of the FXRDs at upper 16° and lower 20° are similar, so the measured fluxes are very close. Because the measured radiation flux of the FXRD at upper 16° comes mainly from the hohlraum wall, the M-band flux of upper 16° is obviously lower than that of upper 64°. For the FXRDs at upper and lower 42°, there are few hohlraum wall areas since both FXRDs look through the octahedral spherical hohlraum from two adjacent LEHs. So the measured radiation fluxes of these two FXRDs are lower than that of upper 16°, which indicates that the emissions of ablated plasmas are weaker than the hohlraum
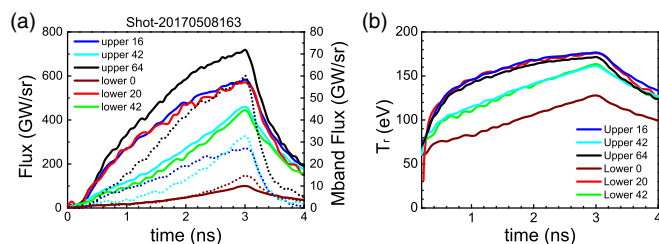
FIG. 4. (a) The temporal behaviors of total radiation fluxes measured by the FXRDs (solid lines) and M-band fluxes measured by the MXRDs (dotted lines). (b) The temporal radiation temperatures derived by using the measured fluxes of different FXRDs.

wall. In fact, the hohlraum wall area in the view field of the FXRD at upper 42° is slightly larger than that of lower 42°, and so the measured radiation flux of upper 42° is slightly higher than that of lower 42°. However, the corona plasmas between the two adjacent LEHs inside the hohlraum contribute much M-band flux to the MXRD at upper 42°, especially before the laser pulse ends. As for the FXRD and MXRD at lower 0°, the measured radiation flux comes mainly from the ablated plasmas near the lower LEH and the accumulated plasmas between the upper and lower LEHs inside the hohlraum, so the measured fluxes are obviously lower than those of other FXRDs and MXRDs.

For a hohlraum with 2 LEHs, a radiation temperature can be derived by using the measured radiation flux [32,33,35,41],

$$T_r = \left(\frac{\pi F_{\mathrm{XRD}}}{\sigma A_{\mathrm{LEH}} \cos \theta} \right)^{0.25}, \quad (1)$$

where T_r is the radiation temperature, F_{XRD} is the measured radiation flux, σ is the Stefan-Boltzmann constant, A_{LEH} is the area of LEH through which the radiation leaves the hohlraum, and θ is the angle between the LEH and FXRD. The purpose of defining a radiation temperature is to evaluate the intensity of radiation field inside the hohlraum, which is crucial for ignition capsule design [27,35,47]. In Eq. (1), a basic assumption, that the hohlraum is a blackbody radiation source, is used. In addition, Eq. (1) is suitable for the case of only one LEH in the view field of FXRD. In fact, the hohlraum is not an ideal blackbody radiation source due to the corona plasmas and laser spots inside the hohlraum [32,35], so the radiation temperature derived in Eq. (1) is just an equivalent temperature but not the real temperature inside the hohlraum [48]. Nevertheless, a radiation temperature can also be derived in a similar way as Eq. (1) even though there is more than one LEH in the view field of the FXRD,

$$T_r = \left[\frac{\pi F_{\mathrm{XRD}}}{\sum_i^N \sigma A_{\mathrm{LEH}}^{(i)} \cos \theta_i} \right]^{0.25}, \quad (2)$$

where N is the number of LEHs in the view field of the FXRD, $A_{\mathrm{LEH}}^{(i)}$ is area of the ith LEH, and θ_i is angle between the ith LEH and FXRD. In Fig. 4(b), we present the radiation temperatures derived from the measured radiation fluxes. As shown in Fig. 4(b), the temporal behaviors of radiation temperatures of upper 16°, 64°, and lower 20° are almost the same. The radiation temperatures raise quickly before 2 ns, which indicates that the contribution of laser spots to the radiation temperatures is relatively large. After 2 ns, the radiation temperature climbs to the peak slowly, indicating that the hohlraum wall contributes more fluxes to the FXRDs at upper 16°, 64°, and lower 20°. Because the measured radiation fluxes of the FXRDs at upper 16°, upper 64° and lower 20° contain not only the emissions

from hohlraum wall, but also the emissions from laser spots and corona plasmas, the derived radiation temperatures may be close to the real radiation temperature inside hohlraum. However, the temporal behaviors of radiation temperatures of upper and lower 42° are different from that of upper 16°. The radiation temperatures of upper and lower 42° increase at almost a constant velocity after 0.6 ns. The reason is that the ablated plasmas near the LEH region and the accumulated plasmas inside the hohlraum contribute major radiation fluxes to these two FXRDs. The longer time, the more ablated plasmas from LEHs and hohlraum wall enter into the view fields of these two FXRDs at upper and lower 42°. For the same reason, the radiation temperature of lower 0° also increases at a constant velocity after 0.6 ns.

The peak radiation temperature inside the octahedral spherical hohlraum is determined by using the shock wave technique with witness material Al. In Fig. 5(a), we present the peak radiation temperatures determined by the shock wave technique and derived from the measured fluxes of the FXRDs at upper 16°, 64°, and lower 20°. As shown in Fig. 5(a), the peak radiation temperature inside the octahedral spherical hohlraum is about 175 eV at 71 kJ, this temperature falls in the range of radiation temperatures of the FXRDs at upper 16°, 64°, and lower 20°. The peak radiation temperatures of the FXRDs at upper 16°, 64°, and lower 20° range from 170 eV to 182 eV at 71 kJ to 84 kJ.

In order to obtain the hohlraum conversion efficiency, the experiment is numerically simulated by using our two-dimensional radiation hydrodynamic code LARED-INTEGRATION [32,36,49] based on the energy balance model [1,9,32]. LARED employs an average atom model and the electron heat flux limit model with a flux limiter of 0.1 [36]. In the numerical simulation, we adopt the model of a spherical hohlraum with two LEHs [50]. The 2-LEH
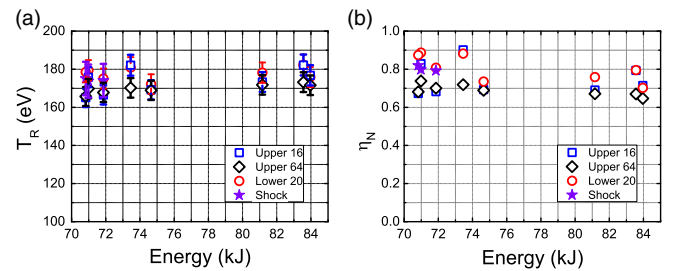
FIG. 5. (a) The peak radiation temperatures determined by the shock wave technique (violet stars) and derived from the measured fluxes of the FXRDs at upper 16° (blue hollow squares), upper 64° (black hollow diamonds), and lower 20° (red hollow circles). (b) The nominal conversion efficiencies obtained by comparing the simulated radiation temperature with the measured radiation temperatures. The blue squares, black diamonds, red circles, and violet stars are the conversion efficiencies calculated by using the radiation temperatures measured by the FXRDs at upper 16°, 64°, lower 20°, and the radiation temperature determined by the shock wave technique, respectively.

spherical hohlraum has the same wall area and LEH area as the octahedral spherical hohlraum. Because LARED cannot properly simulate the octahedral spherical hohlraum, we define a nominal conversion efficiency η_N [32] to evaluate the real hohlraum conversion efficiency,

$$\eta_N = \eta_{\text{sim}} \frac{E_{\text{sim}}}{E_{\text{exp}}}, \qquad (3)$$

where η_{sim} is the simulated conversion efficiency of the code, E_{sim} is the input laser energy in the simulation, and E_{exp} is the measured laser energy coupled the hohlraum in the experiment. The nominal conversion efficiency can be obtained by adjusting the input laser energy so that the simulated radiation temperature is equal to the measured temperature. In Fig. 5(b), we present the nominal conversion efficiencies of the gas-filled octahedral spherical hohlraum for all experimental shots. As indicated in Fig. 5(b), the conversion efficiency from laser into soft x rays of the octahedral spherical hohlraum is in the range from 65% to 90%. However, the conversion efficiency is about 80% if we conclude that the radiation temperature determined by the shock wave technique is more close to the temperature inside the hohlraum.

In conclusion, the first octahedral spherical hohlraum energetics experiment is accomplished at the SGIII laser facility. For the first time, the 32 laser beams are injected into the octahedral spherical hohlraum through six LEHs. In order to obtain comprehensive data of the octahedral spherical hohlraum, the radiation flux streaming out of the LEHs is measured by six FXRDs and four MXRDs placed at different locations of the target chamber. The measured radiation fluxes of different FXRDs and MXRDs are related to their view fields. Assuming the hohlraum is a blackbody radiation source, an equivalent radiation temperature is derived by using the measured radiation flux of the FXRD. For the octahedral spherical hohlraum used in the experiment, the measured radiation temperature of FXRDs is in the range from 170 eV to 182 eV at drive energies from 70 kJ to 84 kJ. For the square laser pulse of 3 ns, the conversion efficiency of the gas-filled octahedral spherical hohlraum from laser to soft x rays is about 80% according to the two-dimensional numerical simulations.

*huo_wenyi@iapcm.ac.cn
†lan_ke@iapcm.ac.cn

[1] J. D. Lindl, Phys. Plasmas 2, 3933 (1995).
[2] S. Atzeni and J. Meyer-ter-Vehn, The Physics of Inertial Fusion (Oxford Science, Oxford, 2004).
[3] H. F. Robey et al., Phys. Rev. Lett. 108, 215004 (2012).
[4] A. J. Mackinnon et al., Phys. Rev. Lett. 108, 215005 (2012).
[5] H. F. Robey et al., Phys. Rev. Lett. 111, 065003 (2013).
[6] V. A. Smalyuk et al., Phys. Rev. Lett. 111, 215001 (2013).
[7] J. Lindl, O. Landen, J. Edwards, E. Moses, and NIC Team, Phys. Plasmas 21, 020501 (2014).
[8] O. A. Hurricane, D. A. Callahan, D. T. Casey, P. M. Celliers, C. Cerjan, E. L. Dewald, T. R. Dittrich, T. Döppner, D. E. Hinkel, L. F. Berzak Hopkins, J. L. Kline, S. Le Pape, T. Ma, A. G. MacPhee, J. L. Milovich, A. Pak, H.-S. Park, P. K. Patel, B. A. Remington, J. D. Salmonson, P. T. Springer, and R. Tommasini, Nature (London) 506, 343 (2014).
[9] L. F. Berzak Hopkins et al., Phys. Rev. Lett. 114, 175001 (2015).
[10] T. Döppner et al., Phys. Rev. Lett. 115, 055001 (2015).
[11] V. N. Goncharov et al., Phys. Plasmas 21, 056315 (2014).
[12] S. P. Regan et al., Phys. Rev. Lett. 117, 025001 (2016).
[13] C. J. Forrest, P. B. Radha, J. P. Knauer, V. Yu. Glebov, V. N. Goncharov, S. P. Regan, M. J. Rosenberg, T. C. Sangster, W. T. Shmayda, C. Stoeckl, and M. Gatu Johnson, Phys. Rev. Lett. 118, 095002 (2017).
[14] E. M. Campbell et al., Matter and Radiation at Extremes 2, 37 (2017).
[15] D. A. Callahan et al., Phys. Plasmas 19, 056305 (2012).
[16] R. P. J. Town et al., Phys. Plasmas 21, 056313 (2014).
[17] O. A. Hurricane et al., Phys. Plasmas 21, 056314 (2014).
[18] D. S. Clark, M. M. Marinak, C. R. Weber, D. C. Eder, S. W. Haan, B. A. Hammel, D. E. Hinkel, O. S. Jones, J. L. Milovich, P. K. Patel, H. F. Robey, J. D. Salmonson, S. M. Sepke, and C. A. Thomas, Phys. Plasmas 22, 022703 (2015).
[19] D. E. Hinkel et al., Phys. Rev. Lett. 117, 225002 (2016).
[20] A. Pak et al., Phys. Plasmas 24, 056306 (2017).
[21] L. Divol et al., Phys. Plasmas 24, 056309 (2017).
[22] K. Lan, J. Liu, D. X. Lai, W. D. Zheng, and X. T. He, Phys. Plasmas 21, 010704 (2014).
[23] K. Lan, X. T. He, J. Liu, W. D. Zheng, and D. X. Lai, Phys. Plasmas 21, 052704 (2014).
[24] K. Lan and W. D. Zheng, Phys. Plasmas 21, 090704 (2014).
[25] S. A. Bel'Kov, F. M. Abzaev, A. V. Bessarab, S. V. Bondarenko, A. V. Veselov, V. A. Gaidach, G. V. Dolgoleva, N. V. Zhidkov, V. M. Izgorodin, G. A. Kirillov, G. G. Kochemasov, D. N. Litvin, E. I. Mitrofanov, V. M. Murugov, L. S. Mkhitarian, S. I. Petrov, A. V. Pinegin, V. T. Punin, A. V. Senik, and N. A. Suslov, Laser Part. Beams 17, 591 (1999).
[26] W. Y. Huo, J. Liu, Y. Zhao, W. Zheng, and K. Lan, Phys. Plasmas 21, 114503 (2014).
[27] K. Lan et al., Matter and Radiation at Extremes 1, 8 (2016).
[28] W. Y. Huo et al., Matter and Radiation at Extremes 1, 2 (2016).
[29] Z. C. Li et al., Phys. Plasmas 24, 072711 (2017).
[30] K. Lan et al., Phys. Rev. E 95, 031202(R) (2017).
[31] Y. H. Chen et al., Matter and Radiation at Extremes 2, 77 (2016).
[32] W. Y. Huo et al., Phys. Rev. Lett. 117, 025002 (2016).
[33] R. L. Kauffman, L. J. Suter, C. B. Darrow, J. D. Kilkenny, H. N. Kornblum, D. S. Montgomery, D. W. Phillion, M. D. Rosen, A. R. Theissen, R. J. Wallace, and F. Ze, Phys. Rev. Lett. 73, 2320 (1994).

[34] L. J. Suter, A. A. Hauer, L. V. Powers, D. B. Ress, N. Delameter, W. W. Hsing, O. L. Landen, A. R. Thiessen, and R. E. Turner, Phys. Rev. Lett. **73**, 2328 (1994).

[35] C. Decker, R. E. Turner, O. L. Landen, L. J. Suter, P. Amendt, H. N. Kornblum, B. A. Hammel, T. J. Murphy, J. Wallace, N. D. Delamater, P. Gobby, A. A. Hauer, G. R. Magelssen, J. A. Oertel, J. Knauer, F. J. Marshall, D. Bradley, W. Seka, and J. M. Soures, Phys. Rev. Lett. **79**, 1491 (1997).

[36] W. Y. Huo, G. L. Ren, K. Lan, X. Li, C. S. Wu, Y. S. Li, C. L. Zhai, X. M. Qiao, X. J. Meng, D. X. Lai, W. D. Zheng, P. J. Gu, W. B. Pei, S. W. Li, R. Q. Yi, T. M. Song, X. H. Jiang, D. Yang, S. E. Jiang, and Y. K. Ding, Phys. Plasmas **17**, 123114 (2010).

[37] W. Y. Huo *et al.*, Phys. Rev. Lett. **109**, 145004 (2012).

[38] H. S. Zhang, D. Yang, P. Song, S. Y. Zou, Y. Q. Zhao, S. W. Li, Z. C. Li, L. Guo, F. Wang, X. S. Peng, H. Y. Wei, T. Xu, W. D. Zheng, P. J. Gu, W. B. Pei, S. E. Jiang, and Y. K. Ding, Phys. Plasmas **21**, 112709 (2014).

[39] N. B. Meezan *et al.*, Phys. Plasmas **17**, 056304 (2010).

[40] S. H. Glenzer *et al.*, Phys. Rev. Lett. **106**, 085004 (2011).

[41] J. L. Kline *et al.*, Phys. Rev. Lett. **106**, 085003 (2011).

[42] J. D. Moody *et al.*, Phys. Plasmas **21**, 056317 (2014).

[43] Z. C. Li, X. H. Jiang, S. Y. Liu, T. X. Huang, J. Zheng, J. M. Yang, S. W. Li, L. Guo, X. F. Zhao, H. B. Du, T. M. Song, R. Q. Yi, Y. G. Liu, S. E. Jiang, and Y. K. Ding, Rev. Sci. Instrum. **81**, 073504 (2010).

[44] Y. S. Li, W. Y. Huo, and K. Lan, Phys. Plasmas **18**, 022701 (2011).

[45] W. Zheng, X. Wei, Q. Zhu, F. Jing, D. Hu, X. Yuan, W. Dai, W. Zhou, F. Wang, D. Xu, X. Xie, B. Feng, Z. Peng, L. Guo, Y. Chen, X. Zhang, L. Liu, D. Lin, Z. Dang, Y. Xiang, R. Zhang, F. Wang, H. Jia, and X. Deng, Matter and Radiation at Extremes **2**, 243 (2017).

[46] L. Guo, S. W. Li, J. Zheng, Z. C. Li, D. Yang, H. B. Du, L. F. Hou, Y. L. Cui, J. M. Yang, S. Y. Liu, S. E. Jiang, and Y. K. Ding, Meas. Sci. Technol. **23**, 065902 (2012).

[47] S. W. Haan *et al.*, Phys. Plasmas **18**, 051001 (2011).

[48] O. S. Jones *et al.*, Phys. Plasmas **19**, 056315 (2012).

[49] H. Yong, P. Song, C. L. Zhai, D. G. Kang, J. F. Gu, X. D. Hang, P. J. Gu, and S. Jiang, Commun. Theor. Phys. **59**, 737 (2013).

[50] H. Cao, Y. H. Chen, C. L. Zhai, C. Y. Zheng, and K. Lan, Phys. Plasmas **24**, 082701 (2017).